Propagation Models for Short-Range Wireless Channels with Predictable Path Geometries

A. Domazetovic, L. J. Greenstein, N. B. Mandayam, and I. Seskar,

Wireless Information Network Laboratory (WINLAB), Rutgers University,

73 Brett Road, Piscataway, NJ 08854, USA †

Abstract

We consider wireless data communications and services characterized by short distances, no shadowing, low power and low antenna heights, deployed in places where a high frequency of potential users is expected. An example of such a system (and service) is infostations that can be deployed at toll booths, parking lots and intersections to name a few scenarios. Within such a system, we expect to see a well-defined geometry of base-to-user radio paths as well as a predictable user trajectory, neither of which can be assumed for the wide-area cellular case. This offers the promise of a strong deterministic component of the channel response, in addition to a weaker stochastic component; this is in contrast to a purely stochastic model, as in existing cellular contexts. In this paper, we present a novel modeling approach which combines the two existing ones - deterministic and stochastic - into a deterministic-plus-stochastic approach. We also present the results from measurements we conducted and the corresponding radio channel models, for three typical outdoor scenarios. Both temporal and spatial channel features are presented. Comparisons between predicted and measured behavior show excellent agreement.

Index Terms

Wireless data, Radio propagation, Channel models

† This work is supported in part by the NSF ITR program under Grant No. CCR-0085986 and by the New Jersey Center for Wireless Technologies. This paper was presented in part at IEEE VTC-F 2002, Vancouver, Canada.

I. INTRODUCTION

We consider a wireless data service characterized by a short-path radio channel, with a strong line-of-sight between the transmitter and receiver antennas and a predictable user trajectory within the system coverage area, as in Infostations [1,2]. By abandoning the constraint that data service must be offered anywhere and anytime, as for voice, we can offer data at much higher rates while using fewer system resources. The idea is to scale down the system coverage to the order of tens of meters at most; restrict antenna heights to a few meters; limit transmit power to less than 100 mW, using unlicensed spectrum (e.g., U-NII); and take advantage of the (presumably) well-defined radio channel behavior. Under short-path conditions, however, we are no longer able to use existing radio channel models for simulation and analysis of system performance. The focus here is to offer a new and reliable set of radio channel models for the short-path system of interest.

Infostations are deployed in places where a high volume of potential users is expected to appear during their daily routines, e.g., toll booths, parking lots, intersections, etc. Within each of these situations, we expect that there will always be a strong line-of-sight (LOS) component between user and base antennas and very little or no shadowing. We also expect to see a predictable user behavior, meaning movement along a limited range of loci, e.g., driving in designated car lanes, thus providing us with a well-defined geometry of base-to-user radio paths. None of these features could be assumed for the wide-area cellular case. This conception enables a strongly deterministic radio channel description, in contrast to the purely stochastic ones that apply to wide-area cellular systems. We will show that, using the above assumptions, we can combine the deterministic and stochastic approaches to derive models that reliably estimate the channel response. We will present results from the measurements we conducted and show excellent agreement between predictions and measurements.

This paper is organized as follows: In Section II we outline the modeling approach. In Section III we describe in detail the measurement program we conducted. In Section IV we present measured results for three 'typical' outdoor scenarios, and we compare them with corresponding (determinis-

tic) radio channel models. In doing so, we identify a low-level background scatter, due to trees and other objects, that requires additional modeling. In Section V we present data analysis and results for this background scatter. We conclude in Section VI with a discussion of model applications and limitations.

II. Approach

There are mainly two approaches to radio channel modeling described in the literature today. One is *deterministic*, which is based on ray tracing [3–7]. The main idea here is to divide the region around the transmitting antenna into clusters of rays and then track each ray from the source to the receiver, taking all the reflections and diffractions into account along each distinct ray path. Each of the rays imparts a magnitude, phase and delay to the transmitted signal. At the receiver, all the incoming rays are vectorially combined. For this approach, detailed knowledge about the propagation environment is assumed. This approach has mainly been used for indoor applications, where the positions of walls and ceilings are known and fixed.

The other approach is *stochastic*, which implies measuring a large number of channel responses and statistically modeling the channel behavior from the measured data. For wireless cellular systems, this has been the dominant approach, producing a number of different models for various applications, e.g., [8–14].

In this paper we present the models derived by combining both approaches, i.e., *deterministic-plus-stochastic*. This approach assumes that the geometry of the environment is known, as well as the user behavior (i.e., trajectory) within the system coverage area. Knowing this, we can trace the rays that are dominant from base to user deterministically. The other lower-power rays can be modeled stochastically. For Infostation types of system [1, 2], this is a highly plausible approach.

Since the way electromagnetic waves propagate depends largely on the path geometry, we have elected to distinguish among several different environments, which we refer to as *scenarios*. Specifically, we have identified the kinds of environments in which we expect the Infostations to be de-

ployed, naming them *typical*. Here, we present results for three typical outdoor scenarios: *Open Roadway with Trees, Roadway with Buildings on the Sides,* and *Parking Lot*. For each of these scenarios, we identified the main mode of radio wave propagation, and using the fact that the user position within each scenario is limited to a presumed trajectory, we have postulated the channel response as a function of user position. We do this using simple geometric relations among the objects within the scenario in question.

We have performed measurements in several different locations having topologies corresponding to the scenarios we are modeling. We have used the results from these measurements to confirm or to modify the postulated response. Finally, we have consolidated our findings into a set of channel models, which we present here.

III. MEASUREMENTS

Basic Approach and Rationale - Measurements of multipath channels are generally of two types, namely, frequency-domain techniques (e.g., frequency domain channel sounding) and time-domain techniques (e.g., spread spectrum sliding correlator, direct RF pulse), with both methods generally including complex data (amplitude and phase) [15]. For the channels of interest here, however, much can be achieved using the far simpler method of single-frequency (or continuous-wave (CW)) transmissions and amplitude (power) measurements. This approach is acceptable because the channel consists of a strong LOS path plus a small number of others and no shadowing; thus, its response is highly predictable and measurements are needed solely to test — and refine — the predictions. By making single-frequency measurements at a number of user positions, each representing a different phasor sum of a small number of paths, we can test the model with high reliability.

If a sinusoidal radio wave (single-frequency wave at radian frequency ω_c) is transmitted through a radio channel, it will travel along several paths to the receiver due to reflections and diffractions from the objects within the environment. The received wave is then a vector sum of all the copies of the transmitted wave, each having different magnitude and delay. As the position of a receiver changes

and/or the positions of objects in the environment change, the multipath combination of the waves changes, resulting in fading. By measuring the received power at numerous places, we can determine the peaks, depths and positions of the fades, and all the spatial variations in between. If the measurements confirm the accuracy of our prediction approach based on geometry, reflection coefficients and antenna gain patterns, then we can accurately state the impulse response (or frequency response) of the channel between the base and any other point in the environment. Thus, CW measurements can be used to confirm channel models that might otherwise require broader-band measurements.

Measurement Technique - The measuring equipment setup we used consisted of the following: the transmitter was an oscillator emitting an unmodulated carrier at 5.3 GHz, at a power of 10 mW. It was directly connected to the transmitting antenna. The receiving antenna was directly connected to the spectrum analyzer, which was set to measure the received power at 5.3 GHz. The spectrum analyzer was connected to a personal computer (laptop) via a GPIB (General Purpose Instrument Bus). The computer ran the program which controls the instruments and records the measured data.

There are two distinct kinds of channel variation we sought to characterize. One variation is spatial, as experienced by moving along a path; the other is temporal, resulting from the relative position changes of scattering objects within the environment. We performed two sets of measurements, to characterize these two aspects of the channel. In the first, the 'moving antenna' measurements, the goal was to determine signal gain as a function of receiver position along a specified path; in the second, the 'fixed antenna' measurements, the goal was to measure the time variations of the channel response resulting from wind-blown leaves on trees and bushes and other dynamics of the environment.

Moving Antenna Measurements - For this type of measurement, we used a vehicle carrying the receiver at a constant speed moving past the transmitting antenna along a predefined trajectory. As the vehicle moved, we recorded the spatial variations of the total received power, in dBm. Having a constant sampling rate, and a vehicle moving at constant speed, we could relate the time samples to

equidistant positions along the traveled trajectory.

We also used two types of antennas: omnidirectional and directional, the latter having a 3-dB beamwidth in the H-plane (azimuth plane) of 120^o. Both antennas were vertically polarized. For the directional antenna case, we pointed the mainlobe (boresight) to be perpendicular to the user trajectory. The receiving antenna was omnidirectional in all cases.

Fixed Antenna Measurements - For this type of measurements, we kept the positions of both antennas fixed while recording received power over time periods of 15 minutes. With the transmitter and receiver fixed, there are no channel variations resulting from the direct ray and other rays reflected from large, fixed objects, i.e., ground and buildings. All the variations in this case are the result of scattering from non-fixed objects. We conducted 'fixed antenna' measurements at several positions for each of several environments, as described in Section V.

IV. Results

A. Underlying Relationships

In free space, the power flux density, Ψ_d, emanating from a transmitting source is given by

$$\Psi_d = \frac{P_t G_t(\theta, \phi)}{4\pi d_r^2} = \frac{|E|^2}{\eta}, \tag{1}$$

where P_t is the transmit power in watts, G_t is the transmit antenna gain, θ and ϕ are direction angles (relative to antenna boresight), d_r is the distance from the radiating source in meters, $|E|$ is the magnitude of the electric field component in volts per meter, and η is the intrinsic impedance of the propagating medium in ohms (in free space $\eta = 120\pi$ ohms) [15]. Also, the power received at a distance d_r, $P_r(d_r)$, is the product of the power flux density and the *effective aperture*, A_e, of the receiver antenna, and can be related to the electric field by [15]

$$P_r(d_r) = \Psi_d A_e = \frac{|E|^2}{\eta} A_e. \tag{2}$$

Finally, if E_0 is the E-field at a reference distance $d_r = d_0$ from the transmitter (in the antenna far field), then for $d_r > d_0$, the free space propagating E-field, due to a CW source, can be given by

$$E(d_r, t) = E_0 \frac{d_0}{d_r} \cos\left(\omega_c (t - \frac{d_r}{c})\right), \tag{3}$$

where c is the wave velocity (speed of light in free space) [15].

In order to postulate the channel response, we use the following rationale. From Equation 1, we express the electric field component, E_0, at a reference distance, d_0, from the transmitting antenna (substituting the free-space value for intrinsic impedance, η):

$$|E_0| = \sqrt{30 P_t}\, \frac{1}{d_0}. \tag{4}$$

The quantity E_0 is the input to the model, which traces the propagation of the electric field component of the electromagnetic wave. Here, we omitted the antenna gain, assuming it to be unity, since the actual gain will be considered for each modeled ray separately. We evaluate E_0 choosing $d_0 = 1$ m. For a frequency of 5.3 GHz (the one we measured at), E_0 at $d_0 = 1$ m can be considered to be in the Fraunhofer region, or antenna far field [15].

Having set E_0, we calculate and model the propagation effects that influence the value of the received electric field for each postulated ray separately. At the output of the model, we compute the total received electric field at distance d_t (the ground distance between antennas) as a sum of fields arriving with each modeled ray, and denote it by $E_r(d_t)$. The corresponding received power, $P_r(d_t)$, which is the quantity we measure, is found as (see Equation 2):

$$P_r(d_t) = \frac{A_e}{\eta} |E_r(d_t)|^2. \tag{5}$$

For the effective aperture of the receiving antenna, A_e, we use the formula for omnidirectional case

(unit gain)

$$A_e = \frac{\lambda^2}{4\pi}, \tag{6}$$

since, (just as in Equation 4) antenna gains are considered for each ray separately [15, 16].

B. Scenario 1: Open Roadway with Trees

Description - We imagine this scenario as a typical roadway in suburban or other non-urban environments. There are no large objects (reflectors) in the proximity of base or user. We assume that the base antenna is mounted alongside the road (e.g., on a lamp post), while the user is in his or her car driving past the base. We also imagine that there are trees and bushes present along the roadway, as depicted in Figure 1.

Postulate - As shown in Figure 1, we postulate that the received signal in this scenario is primarily a sum of two components, line-of-sight (LOS) and ground-reflected (GR). To accurately calculate the magnitude and phase of these two components, we need to take into account the variations of the ground reflection coefficient as a function of user position, as well as both the transmitting and receiving antennas' patterns. Assuming phase synchronism with the line-of-sight component, we can express the (postulated) total received electric field, E_r, as:

$$E_r(d_t, t) = E_0 \left[\alpha \cos\omega_c t + \beta \cos\omega_c (t - \tau)\right], \tag{7}$$

where,

$$\alpha = \frac{g_t(\phi_t, \rho_t) g_r(\phi_r, \rho_r) d_0}{d_{\text{LOS}}}, \quad \beta = R^{\text{GR}}(d_t) \frac{g_t(\theta_t, \rho_t) g_r(\theta_r, \rho_r) d_0}{d_{\text{GR}}} \quad \text{and} \quad \tau = \frac{d_{\text{GR}} - d_{\text{LOS}}}{c}. \tag{8}$$

The quantities $g_t(\phi_t, \rho_t)$ and $g_r(\phi_r, \rho_r)$ are transmitting and receiving antenna gains (signal gains, not power gains). The quantities θ, ρ and ϕ are direction angles (relative to antenna boresight), where subscripts r and t stand for *receiving* and *transmitting*, respectively; θ and ϕ are angles in the E-plane

of radiation; and ρ is the angle in the H-plane of radiation. Note that, for an omnidirectional antenna, the gain in the H-plane is uniform for all angles ρ; thus, for the omnidirectional antenna, gains vary only with E-plane angles, i.e., θ and ϕ. The quantity $R^{\text{GR}}(d_t)$ is a ground reflection coefficient for vertical polarization [15] (Ch. 3.5) [17], evaluated for $\epsilon_r = 5$, representing the dielectric constant for concrete; τ is a delay; ω_c is the radian frequency of the wave; d_t is the ground distance between antennas; and LOS denotes *line-of-sight*, while GR denotes *ground-reflected*. Finally, the path difference between the line-of-sight and ground-reflected components ($d_{\text{GR}} - d_{\text{LOS}}$) we refer to as the *excess path*.

Using simple geometric arguments, we can express ϕ and θ as functions of d_t and the base and mobile antenna heights, h_b and h_m, respectively. Since the user trajectory is a straight line (along the roadway) offset from the base by $\delta = 1.5$ m, as depicted in Figure 1, the distance between antennas, d_t, and the distance, d, along the user trajectory are related through $d_t = \sqrt{\delta^2 + d^2}$. Assuming that the antenna heights, their patterns, and the distance between antenna pole and user trajectory (δ) are known in advance, all the above dependencies can be related through a single parameter d, i.e., the distance along the user trajectory. Using the above information, we can compute (deterministic process) the channel response and the corresponding dB path gain, Γ, as

$$\Gamma = 10 \log \left(\frac{P_r}{P_t} \right). \tag{9}$$

Then, at each point along the user trajectory we can compute the total received electric field, using Equations 7 and 8, and the corresponding received power, using Equation 5.

Having defined all the required parameters, we can now plot the predicted path gain vs. distance along the user trajectory, Figure 2. For this computation, the base antenna height, h_b, is 2 m while the mobile antenna height, h_m, is 1.8 m. The total distance traveled by the user is 30 m, $d = 0$ being at a distance δ from the base antenna (see Figure 1). The antenna patterns were quantized to a 1^o-resolution from the vendor supplied graphs [18]. (Note that we are using signal gains, $g(\phi, \rho)$, rather

than power gains, $G(\phi, \rho)$, relating them as $g(\phi, \rho) = \sqrt{G(\phi, \rho)}$.)

Measurements - In order to confirm the above predictions, we conducted moving antenna measurements (described in Section III) in a Scenario 1 environment having the same system parameters (antenna heights, offset, etc.) as in our computation. We repeated the experiment five times each for both directional and omnidirectional antennas at the base site. The recorded path gain vs. distance for each case showed a very high level of repeatability.

By comparing the predicted and measured curves (Figure 2), we see that both have the same shape, and that the position and levels of peaks and fades are accurately predicted. However, on the recorded curve we see a superimposed low-power background process, in the form of 'grassiness', that is not present in the predicted one; this background process therefore needed modeling. To that end, we performed fixed antenna measurements (described in Section III), the results and analysis of which are presented in Section V. We show there that the background process, most probably resulting from wind-blown leaves on trees and bushes and other dynamics of the channel, can accurately be modeled as a zero-mean, time-varying, complex Gaussian process, having a standard deviation that depends on user position.

Model - Introducing this stochastic component, we can finalize the Scenario 1 channel model, depicted in Figure 1. It is the sum of a deterministic (computed) part, namely line-of-sight plus ground-reflected rays, and a stochastic (simulated) part, namely background scatter. The total received electric field then becomes

$$E_r(d_t, t) = E_0 \, [\alpha \, \cos \omega_c t \, + \, \beta \, \cos \omega_c (t - \tau)] + E_0 \, \mu(d_t, t), \tag{10}$$

where $\mu(d_t, t)$ is a zero-mean, complex Gaussian random process that varies with both distance and time. Following Equation 5, the magnitude of $\mu(d_t, t)$ and the rms power, $\sigma^2(d_t)$, received from this

process (empirically modeled by Equation 18) are related by

$$\sigma^2(d_t) = \frac{A_e}{\eta} |E_0|^2 E[|\mu(d_t, t)|^2]. \quad (11)$$

The comparisons of the measured vs. predicted path gain for Scenario 1 is given in Figure 3. We see that predictions and measurements show excellent agreement. We also see that the simulated stochastic process fully accounts for the 'grassiness' in the measured path gain vs. distance curve. This process could be modeled as a tapped delay line with coefficients that vary in time and have rms values that vary with user position. It presents the superpostion of all the additional rays not accounted for through the deterministic modeling. For single-frequency measurements, due to the central limit theorem, this superposition leads to a complex Gaussian process. Since the total power of the process is at least 20 dB below that of the deterministic component, at all distances measured, knowing the details of the tapped delay line structure may not be critical to the system design. This would be the case, for example, when using QPSK modulation. This is due to the fact that for the constant symbol rate, the susceptibility to interference, i.e., the probability of eye closure, increases with the modulation order. Therefore, the details of power delay profile may not be needed for the case, for example, when using QPSK modulation. If, on the other hand, one seeks system performance for high-order modulation schemes, it becomes necessary to characterize the random component in more detail. For such characterizations, broadband measurements must be performed.

For the directional antenna used at the base, we also observed excellent agreement between measured and predicted path gain vs. distance. The slope of the path gain vs. distance curve, in this case, was steeper (falloff of about 30 dB within $\pm$15 m compared to about 20 dB falloff for omnidirectional antenna, Figure 3), due to the antenna beam shaping in the azimuth plane. Since the antenna was mounted with the boresight perpendicular to the user trajectory, the user was within the antenna mainlobe for a few meters about $d = 0$, and outside the mainlobe elsewhere. The user's received power was thus 8 dB higher than for an omnidirectional antenna at $d = 0$, and fell below for all

$|d| > 1.5$ m.

C. Scenario 2: Roadway with Buildings on the Sides

Description - We envision this scenario as a typical street in an urban environment. There are large buildings in the vicinity of the base and user on one or both sides of the street. We assume that the base antenna is mounted on a sidewalk post (e.g., traffic light pole), while the user is in a car driving past the base. We also assume that trees and bushes may be present. This scenario is depicted in Figure 4.

Postulate - We postulate that, for this scenario, a four-ray model is the appropriate one. This is an extension of the Scenario 1 model, having the two additional reflections from the buildings, as shown in Figure 4. The total received electric field is derivable from the geometry and antenna gain patterns. Again, the distance, d, along the trajectory is the only variable parameter in the model. Thus, the received electric field is similar to Equation 7, with two additional rays:

$$E_r(d_t, t) = E_0 \left[\alpha \cos \omega_c t + \sum_{i=1}^{3} \beta_i \cos \omega_c (t - \tau_i)\right], \tag{12}$$

where α and β_1 are the same as α and β in Equation 8, while

$$\beta_2 = R^{\text{clw}}(d_t)\frac{g_t(\phi_t, \rho_t) g_r(\phi_r, \rho_r) d_0}{d_{\text{clw}}}, \quad \beta_3 = R^{\text{ftw}}(d_t)\frac{g_t(\theta_t, \rho_t) g_r(\theta, \rho_r) d_0}{d_{\text{ftw}}}, \quad \text{and} \quad \tau_i = \frac{d_i}{c}. \tag{13}$$

In the above, clw denotes 'closer wall' (behind the base, offset by a) and ftw denotes 'further wall' (oposite the base, offset by b), as shown in Figure 4. The reflection coefficients $R^{\text{clw}}(d_t)$ and $R^{\text{ftw}}(d_t)$ are evaluated using the formulas for horizontal polarization in [15] since, for vertical polarization reflected from vertical walls, the E-field is normal to the plane of incidence; and d_i denotes the path length difference between the i^{th} and line-of-sight rays.

Measurements - To confirm the above picture, we conducted moving antenna measurements in

an environment corresponding to Scenario 2. The base antenna was mounted at 2 m; the mobile antenna was mounted at 1.8 m; the trajectory was again a straight line (along the road) with offset $\delta = 1.5$ m; the closer building was $a = 5$ m behind the base; and the further building was $b = 22$ m away from the user trajetory opposite the base. Both buildings had walls made of brick (dielectric constant, $\epsilon_r = 4.44$ [15, 17]). The total distance traveled by the user was 30 m. As in Scenario 1, for both directional and omnidirectional antennas at the base site, we saw a high level of experiment repeatability. Comparing measured and predicted path gain vs. distance, we could again detect the low-power background scatter, although, due to the additional two rays, the deterministic component alone has increased 'grassiness' compared to Scenario 1. We show in Section V that the detected scatter can be incorporated using the same model as for Scenario 1 (Equation 18).

Model - Having modeled four rays in deterministic fashion, as well as background scatter in stochastic fashion, we can complete the Scenario 2 channel model of Figure 4. The total received electric field becomes

$$E_r(d_t, t) = E_0 \left[\alpha \cos \omega_c t + \sum_{i=1}^{3} \beta_i \cos \omega_c (t - \tau_i) \right] + E_0 \, \mu(d_t, t) \tag{14}$$

where $\mu(d_t, t)$ is a zero-mean, complex Gaussian random process, explained in the prior Scenario 1 discussion. The measured and predicted path gains are plotted together in Figure 5 and, again, show excellent agreement. For the deterministic component, the four rays were computed from our equations, while the background scatter was simulated from our model of the stochastic component.

We can see that the two additional reflections from the building walls introduce only slight differences in path gain vs. distance compared to Scenario 1, but they add increased depth to the 'grassiness' of the plot. As for Scenario 1, the scatter power is at least 20 dB below that of the deterministic component at all distances. Thus, for many applications, knowing its details (e.g., power delay profile) is not required.

In cases where the symbol rate is high, the rms delay spread of the channel can become important,

the product of symbol rate and delay spread being a measure of potential intersymbol interference. For general information purposes, we show in Figure 6 the rms delay spreads for just the deterministic components for Scenarios 1 and 2. We see that for Scenario 1 the rms delay spread is less than a nanosecond for all distances. This is due to the large power difference between the line-of-sight and ground-reflected rays, and due to the small delay between them. For Scenario 2, the rms delay spread increases to the order of 10 ns. This results, especially at larger distances, from the large delays between the rays reflected from the buildings, even though their powers are low and comparable to that of the ground-reflected ray. Thus, even though the wall-reflected rays add little to the power vs. distance curves, they can add significantly to the rms delay spread. The stochastic component will increase the rms delay spread further; therefore, the above numbers are lower-bound estimates.

As in Scenario 1, the path gain vs. distance curve for a directional antenna at the base was steeper (faster falloff). The antenna was mounted with its boresight perpendicular to the user trajectory. Again, the user received more power, within the antenna mainlobe, than for the omnidirectional case. However, the power was not lower outside of the mainlobe. This is probably due to the additional rays reflected from the buildings, which were not present in Scenario 1.

D. Scenario 3: Parking Lot

Description - We picture this scenario as a typical parking lot usually found in front of shopping malls and supermarkets. There are two lines of parked cars followed by the driving lane and then more parked cars. We imagine the base antenna as mounted in the midst of parked cars, possibly on a lamp post; and we imagine the user as driving at slow speed looking for a parking space. This situation is depicted in Figure 7.

Postulate - Scenario 3 has a significantly different geometry than Scenarios 1 and 2. A number of parked cars pose the objects which introduce additional reflections and diffractions, creating stronger multipath combinations of the received signal. Since cars are made mainly of metal and glass, we expect different reflection properties, depending on where the reflections take place. Therefore, we

postulate that, for this scenario, only the line-of-sight (LOS) component can be predicted in a deterministic fashion. All additional reflected and diffracted rays become intractable for deterministic analysis, so we account for them in stochastic fashion. This implies that we can express the total received electric field (deterministic part) as

$$E_r(d_t, t) = E_0\,\alpha\,\cos\omega_c t \quad \text{where,} \quad \alpha = \frac{g_t(\phi_t, \rho_t) g_r(\phi_r, \rho_r) d_0}{d_{\text{LOS}}}. \tag{15}$$

The corresponding received power and path gain are then calculated using Equations 5 and 9, respectively. Again, using simple geometry, we can express all of the above as functions of a single variable, d, i.e., the distance along the user trajectory.

Measurements - Just as for Scenarios 1 and 2, we conducted moving antenna measurements in an appropriate environment for Scenario 3: a mobile antenna height of 1.8 m; a base antenna height ranging between 2 m and 3.5 m; trajectory offsets of $\delta_1 = 6$ m (near the close-in cars); $\delta_2 = 10$ m (middle of the drive lane); and $\delta_3 = 14$ m (near the opposite line of cars); and a total distance traveled by the user of 20 m (see Figure 7). As in the first two scenarios, we also observed a high level of experiment repeatability. It was expected that the predicted and measured curves would differ, but also that the predicted curve would have the same trend as the measured one. In Section V, we show that the predicted path gain vs. distance is approximately the mean of the measured path gain vs. distance. We also show that the fluctuations seen in the recorded curve can be represented as a zero-mean, complex Gaussian process, with standard deviation dependent on user position. Thus, the overall process can be modeled as Ricean, with the specular term being a predictable function of user position and the Ricean K factor (specular power/scatter power) being determined from measurements as a function of position. In Section V, we further show that the K factor is essentially constant over the user trajectory.

Model - Having characterized the stochastic component, we can complete the Scenario 3 channel

model depicted in Figure 7. The total received electric field is

$$E_r(d_t, t) = E_0\,\alpha\,\cos\omega_c t + E_0\,\mu(d_t), \tag{16}$$

where $\mu(d_t)$ is a zero-mean, complex Gaussian random variable with variance $|\alpha|^2/K$, K being constant with position.

The comparison of measured and modeled path gain vs. distance, for an omnidirectional base antenna, is shown in Figure 8. In contrast to Scenarios 1 and 2, the rms scatter is down only one order of magnitude (not two or more) from the deterministic component. This may necessitate more detailed modeling for this scenario (e.g., broadband measurements to quantify the corresponding tapped delay line structure) and it will almost certainly call for adaptive methods to mitigate the effects of the scatter component on system performance.

It is interesting to see how the Ricean K factor depends on system parameters. In Figure 9 we compare the K values versus user trajectory offset. It can be seen that K is maximum in the midle of the road and decreases as the user approaches the parked cars. We also found that increasing the antenna height leads to higher K values. In both analyses, we see that, as the proximity of parked cars decreases, the K factor increases, as expected.

We also observed that the K values measured on different days, though they correspond to the same system conditions, significantly varied. This was probably due to different numbers of parked cars and different traffic conditions. Thus, the value of K depends on the traffic, the density and positions of parked cars, and other environment features. Although we do not provide here a detailed model for the K factor as a function of system/scenario parameters (antenna height, trajectory offset, traffic, etc.), our measurements show that, over all conditions, the K factor lies in a range from 8 dB to 13 dB, with a mean of 10 dB. These values come from 29 experiment trials conducted on 6 different days (parking setups), during 3 seasons (fall, winter and spring), with different traffic intensities, using both directional and omnidirectional base antennas at heights between 2 and 3.5 meters, and

for different trajectory offsets. Therefore, we believe that, for simulation purposes, one can just consider different K factor values from this range, e.g., best (13 dB), worst (8 dB) and mean (10 dB). Similar values for K (in similar scenarios) are also reported in [22].

V. Analysis of the Background Scatter Component

Having postulated the main (deterministic) mode of radio propagation in each scenario we were modeling, we were able to closely predict the shape of the path gain vs. distance curve as well as the depths of the fades. However, the 'grassiness' of the measured curves is not accounted for by this deterministic modeling (see Figure 2). We postulate that the 'grassiness' is due to additional reflectors, which cause additional spatial variation of the total received power. We further postulate that (for Scenario 1 and 2) the reflectors are the leaves and branches of surrounding trees, which move in the wind. If correct, we can estimate the extent of this scatter by making fixed antenna measurements (described in Section III) over time at different points along the user path. We find that the mean square time fluctuations so measured fully account for the observed 'grassiness'. For Scenario 3, we postulate that the spatial variation of the received power is due to reflections and diffractions from the parked cars. We present a way to model this scatter as well.

A. Statistics of the Measured Signal over Time (Scenarios 1 and 2)

Our first task was to determine the probability distribution of the received signal envelope over time. We compared the cumulative distribution functions (CDFs) of several standard distributions against the CDF of the measured data. We found that the received power can be modeled as the square (i.e., the power) of a Ricean process.

For the estimation of the Ricean K factor in all our analyses we used the moment method of [19]. It follows that the received signal can be represented as:

$$g(t) = V + v(t), \tag{17}$$

where V is the mean received signal amplitude and $v(t)$ is a time-varying, zero-mean, complex Gaussian process [8]. The envelope of $g(t)$, that is, $|g(t)|$, is a Ricean process, with K factor $|V|^2/E[|v(t)|^2]$.

B. Model of the Scatter Power Versus Distance

Having determined that the received signal power, $|g(t)|^2$, can be modeled as the power of a Ricean process, we sought to model the dependence of the scatter power, $E[|v(t)|^2] = \sigma^2$, on distance. We performed extensive measurements at twenty one different positions along one Scenario 1 trajectory, including the effect of antenna directivity on the scatter power. We found that the results are quite similar for both antennas (similar slope, intercept and rms deviation). Therefore, we used only omnidirectional antenna measurements to model σ^2 versus distance.

In another experiment, we measured σ^2 at six positions along each of four distinct paths. The results are summarized in Figure 10, which shows the distance dependence of σ^2/P_t, i.e., the normalized scatter power, since the goal was to derive a model not dependent on the transmit power, P_t. The four environments, representing both Scenarios 1 and 2, had different densities of trees and bushes in the near surroundings. As is shown, the data do not change much across environments and the fit derived by pooling all the data can be used as a model for the scatter power in any similar envoronment (with similar values for base and mobile antenna heights, i.e., on the order of a few meters). The rms deviation of all points about this fit is only 1.8 dB. In other words, we can use a single model for σ^2/P_t vs. d_t (in meters) for Scenarios 1 and 2, namely,

$$10\log\left(\frac{\sigma^2}{P_t}\right) = -78 \; - \; 0.6 \; [10\log(d_t)]\,, \tag{18}$$

where d_t, the ground distance between antennas, is related to d, the distance along the user trajectory, by $d_t^2 = d^2 + \delta^2$.

We also analyzed the sprectrum of the time varying process whose power is σ^2. The estimate of the power spectral density is presented in [20, 21].

C. Scatter Component for Scenario 3

In Scenario 3, the recorded path gain vs. distance showed significant fluctuations about the predicted power of the line-of-sight component. We postulate that these fluctuations result from the superposition of multiple reflections and diffractions from parked cars, which change (both in magnitude and phase) as the user moves along its trajectory. In order to confirm this, we performed fixed antenna measurements. We determined that the variations are not due to time changes in the environment, such as wind-blown leaves as in Scenarios 1 and 2, since the rms value of the channel time variations was an order of magnitude below that recorded over distance. Therefore, we conclude that the fluctuations are due to user movements in an environment with many fixed scatterers (i.e., parked cars).

Normalizing the recorded path gain vs. distance by the line-of-sight component power (subtraction on a dB scale), we found that the fluctuations were fairly equal along the whole trajectory, and that they could be modeled as due to an additive, zero-mean, complex Gaussian process. Thus, the overall process is Ricean. In general, the scattering process can be represented by a tapped delay line structure whose gain coefficients change with user position but are not time-varying. To determine the details of this structure, broadband measurements would be required.

The conclusion of the above analysis is that the scatter component at the output in Figure 7 has a mean-square value $|\alpha|^2/K$, where α depends on the user distance along its trajectory but K is essentially independent of it. The dependence of K on other factors, such as trajectory offset, is discussed in Section IV.

VI. CONCLUSION

We have presented a novel approach to radio channel modeling that can be applied to short-path channels with well-defined geometries, such as Infostations. In contrast to existing channel models, which are either deterministic or stochastic, we have derived a simple deterministic-plus-stochastic modeling approach using ray analysis and CW measurements. The ray analysis was used to predict

the deterministic component of the channel response as a function of user position; the measurements were used to derive empirical models for the stochastic component and to confirm the overall approach. The modeling was facilitated through the classification of the physical environments into three different categories, corresponding to three different user/Infostation scenarios.

The measurements we performed were highly repeatable, showing little variation from time to time and place to place. We measured temporal variations in addition to the variations of the channel response with user position. We also studied, for each scenario, the effects of antenna directivity on the channel response; and, for the highest-scatter case (Scenario 3), we looked at the impact of antenna height and path geometry on relative scatter power.

For Scenarios 1 and 2, we determined that the rms scatter is at least 20 dB below the deterministically predicted components. This implies that for low-order modulation schemes (e.g., QPSK), knowing the details of the scatter process, and using measures to counter it, may not be required. If, however, higher-order modulation schemes are desired, this will call for adaptive schemes to mitigate the multipath scatter. For the design and analysis of these schemes, the structure of the scatter process (e.g., the number of paths, delays and rms gains) may need modeling; to this end, broadband measurements would be required. For Scenario 3, where the channel is Ricean, with K factors as low as 10 dB (or less), some adaptive schemes (e.g., equalization, power control, channel estimation, etc.) will certainly be necessary. Again, the structure of the multipath scatter may have to be known in greater detail, and this would necessitate broadband measurements.

Regarding what specific features of the scatter process need to be known, this depends on the radio technique and the performance requirements. Relevant issues include the mode of access (single-carrier, OFDM, CDMA, etc.), the type of modulation (BPSK, QPSK, 16-QAM, etc.), the kinds of mitigating techniques (equalization, Rake, diversity, etc.), and the required bit (or block) error rate. In any case, by showing the predictable deterministic component to be dominant in typical Infostation scenarios, *and* by modeling the rms scatter, we have significantly narrowed both the amount

of further channel detail required and the range of conditions requiring it. Indeed, in some cases, from the scenario geometry, very reasonable conjectures about the unknown channel features (e.g., rms delay spread) may suffice to assess the impact of the scatter component, avoiding the need for broadband measurements and modeling.

REFERENCES

[1] R. D. Yates and N. B. Mandayam, "Challenges in Low-Cost Wireless Data Transmission," *IEEE Signal Processing Magazine*, Vol. 17, No. 3, pp. 93-102, May 2000.

[2] R. H. Frenkiel, B. R. Badrinath, J. Borras and R. D. Yates, "The Infostations Challenge: Balancing Cost and Ubiquity in Delivering Wireless Data," *IEEE Personal Communications*, Vol. 7, No. 2, pp. 66-71, April 2000.

[3] R. A. Valenzuela, "A Ray Tracing Approach to Predicting Wireless Transmission," *Proceedings 43rd IEEE Vehicular Technology Conference*, pp. 214-218, 1993.

[4] R. A. Valenzuela, L. J. Greenstein, "Performance evaluations for urban line-of-sight microcells at 900 MHz using a multi-ray propagation model," *Global Telecommunications Conference GLOBECOM*, Vol. 3, pp. 1947-1952, 1991.

[5] K. Seong-Cheol, B. J. Guarino Jr., T. M. Willis III, V. Erceg, S. J. Fortune, R. A. Valenzuela, L. W. Thomas, J. Ling, J. D. Moore, "Radio propagation measurements and prediction using three-dimensional ray tracing in urban environments at 908 MHz and 1.9 GHz," *IEEE Transactions on Vehicular Technology*, Vol. 48, No. 3, pp. 931-946, May 1999.

[6] S. Y. Seidel, T. S. Rappaport, "Site-specific propagation prediction for wireless in-building personal communication system design," *IEEE Transactions on Vehicular Technology*, Vol. 43, No. 4, pp. 879-891, April 1994.

[7] S. Y. Seidel, T. S. Rappaport, "A ray tracing technique to predict path loss and delay spread inside buildings," *Global Telecommunications Conference*, Vol. 2, pp. 649-653, 1992.

[8] V. Erceg, L. J. Greenstein, S. Y. Tjandra, S. R. Parkoff, A. Gupta, B. Kaulic, A. A. Julius and R. Bianchi, "An Empirically Based Path Loss Model for Wireless Channels in Suburban Environments," *IEEE Journal on Selected Areas in Communications*, Vol. 17, No. 7, pp. 1205-1211, July 1999.

[9] COST 231 Final Report, *Digital Mobile Radio Towards Future Generation Systems*.

[10] L. J. Greenstein, V. Erceg, Y. S. Yeh, M. V. Clark, "A new path-gain/delay-spread propagation model for digital cellular channels" *IEEE Transactions on Vehicular Technology*, Vol. 46, No. 2, pp. 477-485, February 1997.

[11] Hata, Masaharu, "Empirical formula for propagation loss in land mobile radio services," *IEEE Transaction on Vehicular Technology*, Vol. 29, No. 3, pp. 317-325, March 1980.

[12] H. Asplund, A. F. Molisch, M. Steinbauer, N. B. Mehta, "Clustering of scatterers in mobile radio channels - evaluation and modeling in the COST259 directional channel model", *IEEE International Conference on Communications, ICC 2002*, Vol. 2, pp. 901-905, 2002.

[13] J. B. Andersen, T. S. Rappaport, S. Yoshida, "Propagation measurements and models for wireless communications channels" *IEEE Communications Magazine*, Vol. 33, No. 1, pp. 42-49, January 1995.

[14] S. Y. Seidel, T. S. Rappaport, S. Jain, M. L. Lord, R. Singh, "Path loss, scattering and multipath delay statistics in four European cities for digital cellular and microcellular radiotelephone," *IEEE Transactions on Vehicular Technology*, Vol. 40, No. 4, pp. 721-730, April 1991.

[15] T. S. Rappaport, *Wireless Communications - Principles and Practice*, Prentice Hall, 1996.

[16] J. D. Kraus, *Antennas*, McGraw-Hill, 1988.

[17] O. Landron, M. J. Feuerstein, and T. S. Rappaport, "A Comparison of Theoretical and Empirical Reflection Coefficients for Typical Exterior Wall Surfaces in a Mobile Radio Environment," *IEEE Transactions on Antennas and Propagation*, Vol. 44, No. 3, pp. 341-351, March 1996.

[18] Cushcraft Communications Antennas, ISM Band Antennas, *Product Data Sheet*, 2001.

[19] L.J. Greenstein, D.G. Michelson, and V. Erceg, "Moment-Method Estimation of the Ricean K-Factor," *IEEE Communication Letters*, Vol. 3, No. 6, pp. 175-176, June 1999.

[20] A. Domazetovic, L.J. Greenstein, N. B. Mandayam, I. Seskar, "Estimating the Doppler Spectrum of a Short-Range Fixed Wireless Channel," *IEEE Communication Letters, Submitted*.

[21] A. Domazetovic, L.J. Greenstein, N. B. Mandayam, I. Seskar, "A New Modeling Approach for Wireless Channels With Predictable Path Geometries," *VTC Fall 2002 Conference Proceedings, To appear*.

[22] J. S. Davis, II and J. P. M.G. Linnartz, "Vehicle to Vehicle RF Propagation Measurements," *Conference Record of the Twenty-Eighth Asilomar*, Vol. 1, pp. 470-474, 1994.

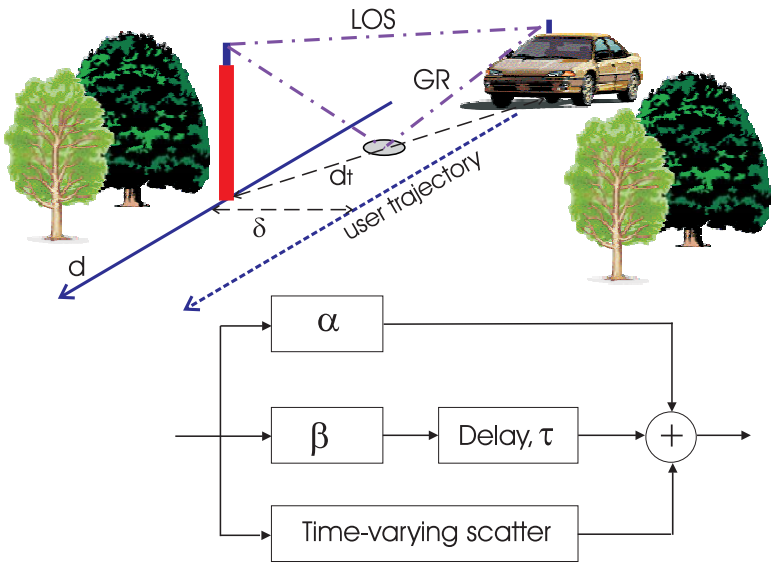

Fig. 1. Scenario 1: Open roadway with trees - description and channel model

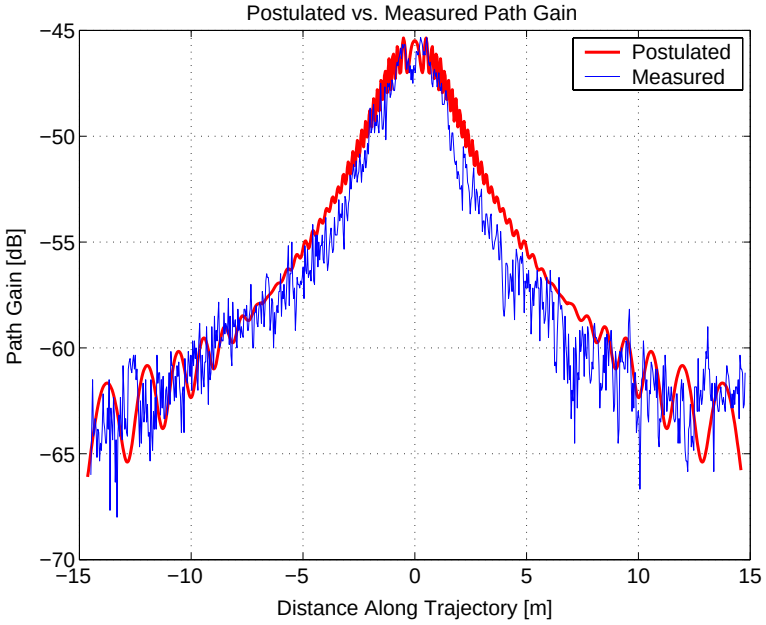

Fig. 2. Comparing postulated and measured path gain vs. distance for Scenario 1

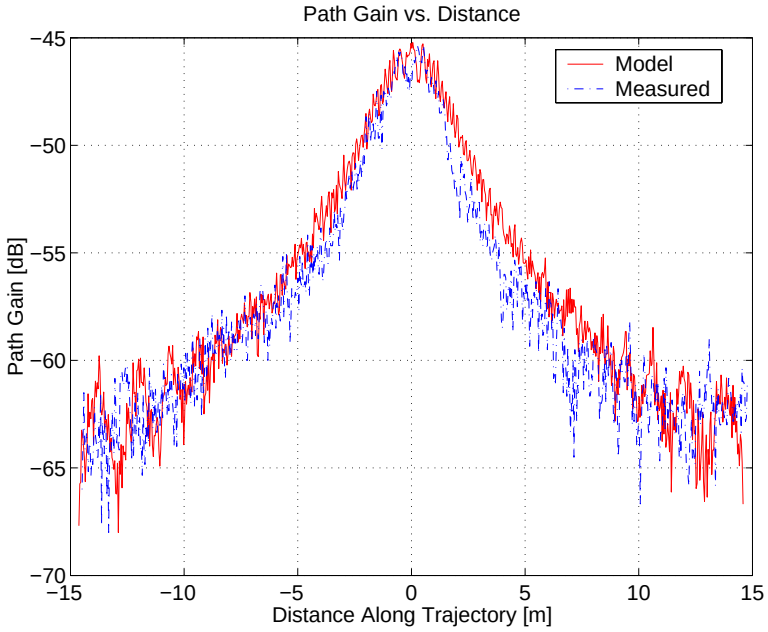

Fig. 3. Path gain vs. distance for Scenario 1: Measured vs. predicted

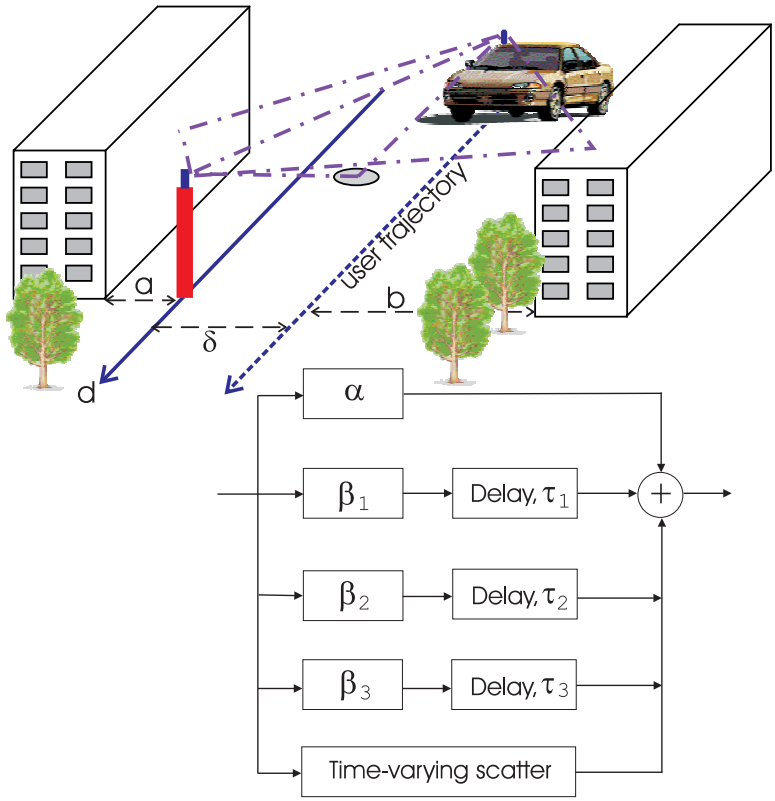

Fig. 4. Scenario 2: Roadway with buildings on the sides - description and channel model

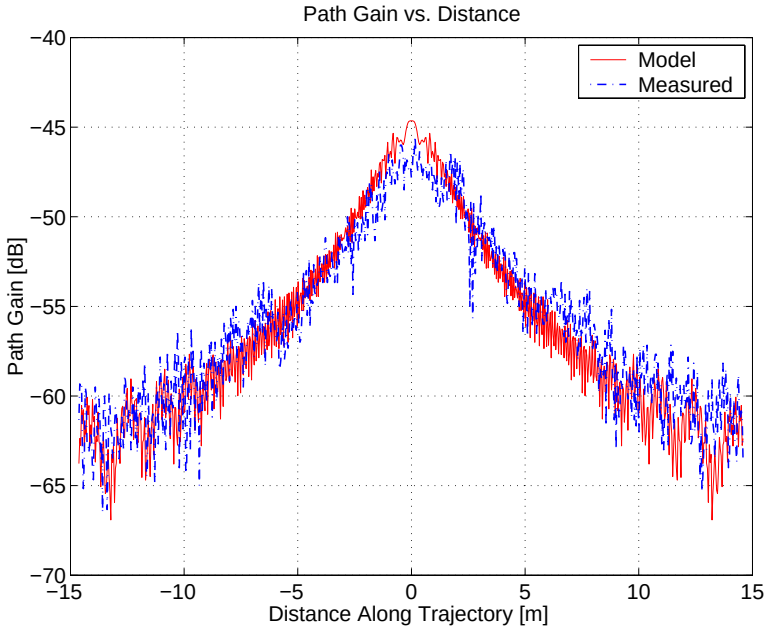

Fig. 5. Path gain vs. distance for Scenario 2: Measured vs. predicted

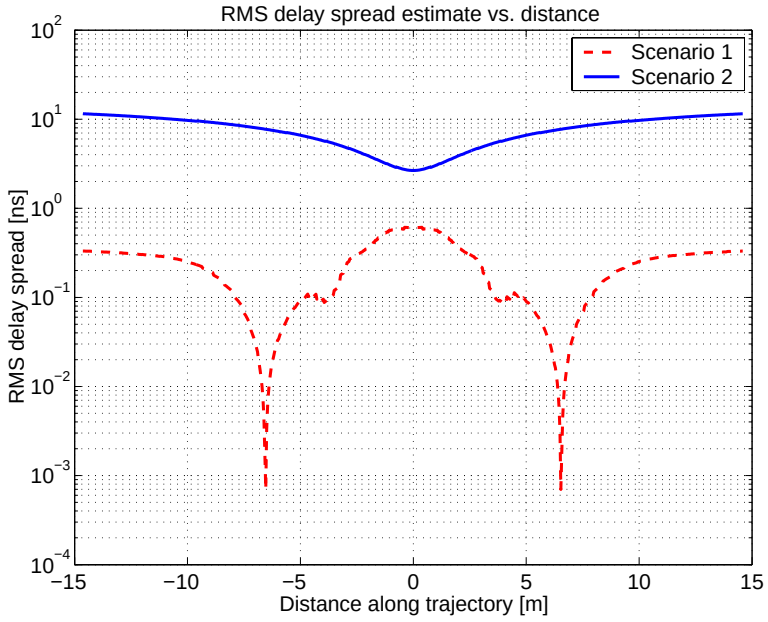

Fig. 6. rms delay spread estimate for Scenarios 1 and 2

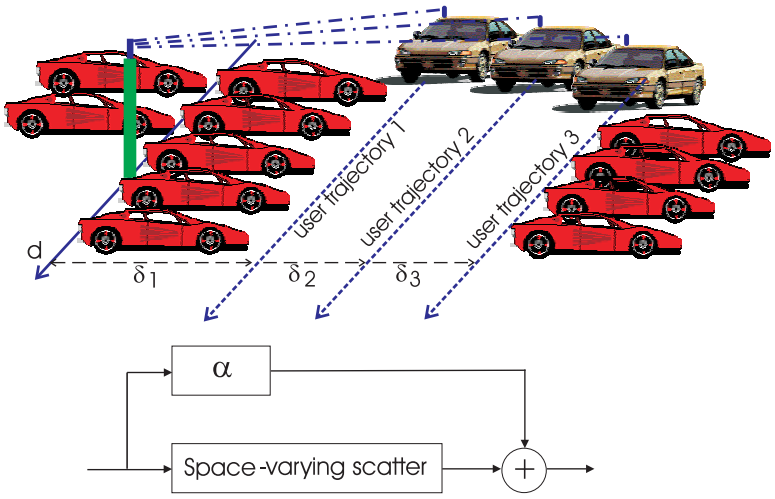

Fig. 7. Scenario 3: Parking lot - description and channel model

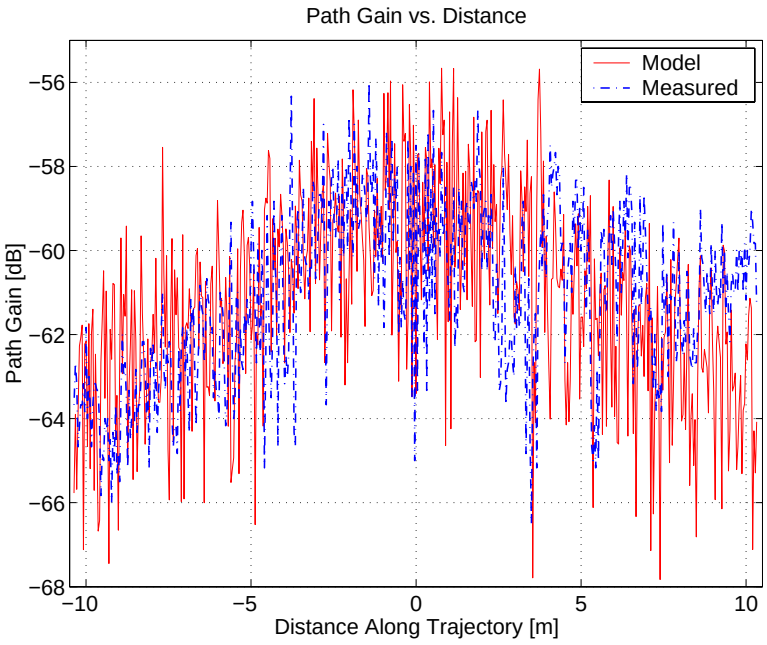

Fig. 8. Path gain vs. distance for Scenario 3: Measured vs. predicted

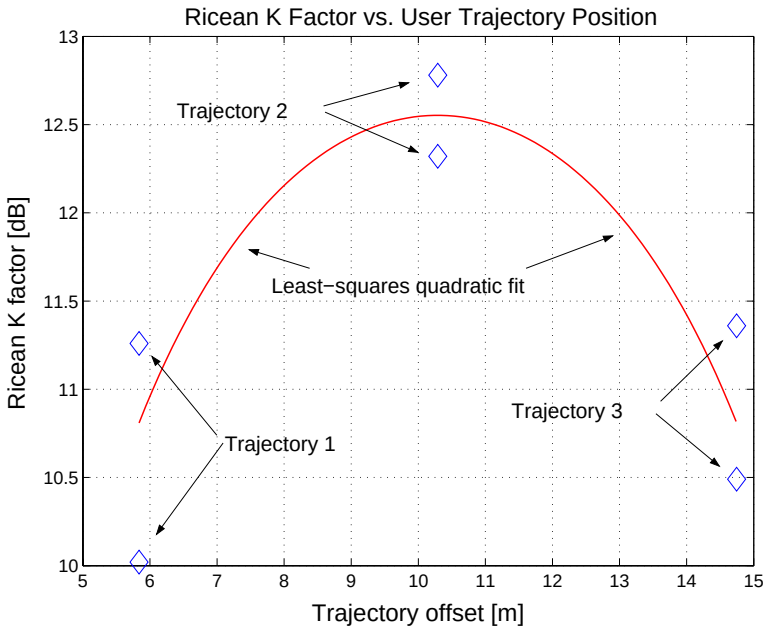

Fig. 9. Scenario 3: Ricean K factor vs. trajectory offset

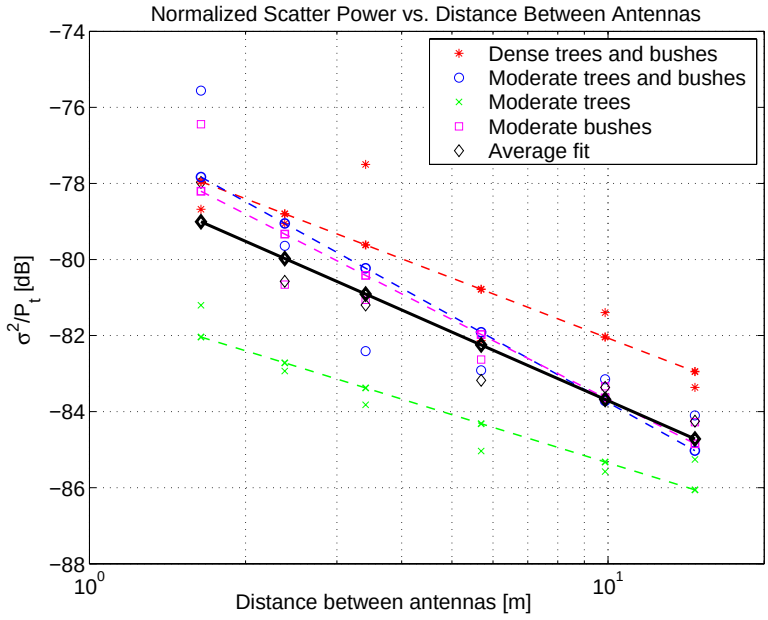

Fig. 10. Normalized scatter power vs. distance